Macromolecules

ARTICLE

pubs.acs.org/Macromolecules

Ionic Purity and Connectivity of Proton-Conducting Channels in Fluorous-Ionic Diblock Copolymers

Emily Ming Wai Tsang, Zhiqing Shi,† and Steven Holdcroft*

Department of Chemistry, Simon Fraser University, Burnaby, BC V5A 1S6, Canada

Supporting Information

ABSTRACT: Diblock copolymers of sulfonated poly([vinylidene difluoride-*co*-hexafluoropropylene]-*b*-styrene) [P(VDF-*co*-HFP)-*b*-SPS] were prepared for the purpose of studying the role of ionic purity and connectivity on proton exchange membranes. Block ratios were controlled to provide membranes with different morphologies. Within each membrane series, the ion content was controlled either by varying the length of the fully sulfonated polystyrene (PS) block, or by varying the degree of sulfonation of a fixed PS block. For a given ion exchange capacity (IEC), water uptake and proton conductivity were shown to be significantly influenced by the degree of sulfonation of the PS block and, thus, the ionic purity of the "ion-rich" channels. Fully sulfonated membranes with 6−17 vol % PS possessed disordered ionic clusters (6−20 nm in diameter). Although these membranes show relatively high water sorption at low IEC ranges, their water sorption and proton conductivity are less sensitive to changes in IEC. This reduced their tendency for acid dilution at high ion contents, allowing for a continuous increase in proton conductivity over a greater range of IEC. Partially sulfonated membranes with 35, 45, and 50 vol % PS displayed a lamellar morphology. Water content was found to be lower in the partially sulfonated membranes due to the influence of the nonsulfonated PS host matrix surrounding the ionic aggregates of polystyrenesulfonic acid (PSSA). For a given IEC, partially sulfonated membranes with lower PS contents required relatively high degree of sulfonation, resulting in enhanced connectivity of ionic PSSA aggregates, which, in turn, led to greater water uptake and proton conductivity. This work concludes with the finding that the design of polymers that form well-defined "proton-conducting channels", as determined by electron microscopy, do not necessarily translate to high proton conductivity membranes, as it is the connectivity of the protogenic aggregates within these channels that has the strongest influence on the membrane transport properties.

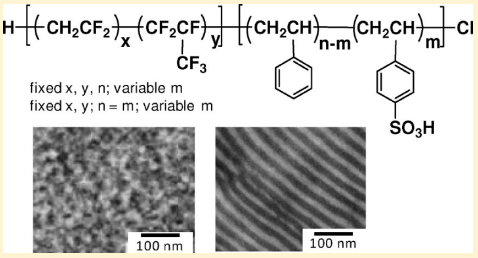

INTRODUCTION

Proton exchange membrane fuel cells (PEMFCs) are low emission, high efficiency, energy conversion devices.[1−3] The proton exchange membrane (PEM) is a crucial component serving as a separator to prevent mixing of reactant gases and as an electrolyte for conducting protons from anode to cathode.[1] The material requirements for a PEM include high proton conductivity, good mechanical and chemical stability, low gas permeability, and low production cost.[2,4,5]

State-of-the-art membranes are based on perfluorosulfonic acid (PFSA) ionomers. PFSA membranes offer high proton conductivity under fully hydrated conditions, excellent mechanical strength, and long-term stability in both oxidative and reductive environments. However, high production cost, vulnerability to dehydration, poor fuel barrier properties, and emerging issues about recycling are major concerns in the use of PFSA membranes in the mass commercialization of PEMFCs. Over the past decade, attention has been focused on the design of alternative PEM materials prepared at lower cost and with improved properties.[2,4−7] Although a wide variety of novel polymer systems have been studied for this purpose, there is yet a comprehensive understanding of fundamental structure−property relationships in PEMs. In particular, the role of polymer microstructure on the morphology and, subsequently, on the physicochemical properties of membranes are subjects of much research interest.[8−11]

The nanostructure and morphology of membranes are believed to play a profound role on their proton conduction.[8] The morphology of Nafion membranes, for example, has been characterized as possessing an interconnected network of nanometer-sized ionic channels in a fluorocarbon matrix.[12−16] Proton conduction occurs through hydrophilic ionic channels, wherein protons dissociate and are mobilized by water molecules.[15,17] However, it is not fully understood how the polymer microstructure affects ionic aggregation and connectivity of ionic domains, and how the membrane morphology influences water sorption and proton conductivity. In this context, model polymers that form distinct but variable morphological structures are useful for elucidating structure−property relationships and for gaining insights into optimal structures for membrane design.

It is well-established that block copolymers, having immiscible segments, self-assemble into a range of ordered, periodic structures through the process of microphase separation.[18,19] The enthalpy of demixing of incompatible segments provides the

Received: May 6, 2011
Revised: August 5, 2011
Published: October 28, 2011

driving force for microphase separation in block copolymers, while further separation into macroscopic domains is prevented by chemical bonding between segments. The extent of phase separation and the resulting morphological structures are dependent upon several parameters such as chemical dissimilarity between blocks, length of each block, block ratio, and crystallinity.

The high-level of morphological control renders block copolymer ionomers potentially useful for studying structure−property relationships in PEMs, and these are the subject of a recent review by Elabd and Hickner.[20] Block ionomers for PEM materials are typically comprised of an ionic and a nonionic block. This is often achieved by having constituent blocks to be composed of chemically different units, or of units that are chemically identical except that one block is sulfonated and the other is not. Chemical immiscibility between the constituent blocks induces phase separation of ion and nonionic domains, wherein proton transport is facilitated by the ionic domain while mechanical strength is provided by the nonionic domain. Well-defined sulfonated block copolymers can yield ordered nanostructures with tailored morphologies and domain sizes and thus, allow for an investigation of the effects of morphology and molecular order on proton transport.

The morphology and properties of PEMs based on polystyrenesulfonic acid-containing block ionomers have been extensively studied.[21−43] Partially sulfonated poly(styrene-*b*-[ethylene-*co*-butylene]-*b*-styrene) (S-SEBS), possessing a sequence of ionic/nonionic/ionic block, have been investigated for elucidating structure−property relationships as well as the potential application as low-cost membranes in hydrogen PEMFCs.[21−35] It is reported that different morphologies can be obtained for S-SEBS when membranes are cast from different solvents, and proton conductivities is highly dependent upon membrane morphologies.[28,34] Elabd and co-workers[37−40] examined a similar triblock copolymer, partially sulfonated poly(styrene-*b*-isobutylene-*b*-styrene) (S-SIBS), which is also found to adopt different morphologies that are dependent upon the casting solvent. Proton conductivity (in-plane direction) is significantly higher in membranes with lamellar structure compared to those with disordered structure. In addition, S-SIBS exhibits a change in morphology with increasing ion contents.[40] Hickner and co-workers[44] have prepared midblock-sulfonated triblock copolymers to investigate how the location of the sulfonated block as well as the chemical composition of the nonionic blocks influence proton transport properties. ABA triblocks with an ionic center block comprising of sulfonated polystyrene and nonionic outer blocks comprising of poly(hexyl methacrylate) (PHMA) were found to provide higher proton transport compared to their partially fluorinated analogue (i.e., nonionic outer blocks consisting of poly(perfluorooctyl methacrylate). This is presumably due to the lower glass transition temperature (T_g) and higher solubility of the hydrocarbon PHMA block in the casting solvent, which led to a greater degree of morphological order.

Balsara and co-workers[45] have reported an extensive morphological study of sulfonated poly(styrene-*b*-methylbutylene) (PSS-*b*-PMB) to determine the effects of molecular weight, sulfonation level, and temperature on their phase behavior. It was observed that PSS-*b*-PMB, despite having a narrow PSS volume fraction of 0.45−0.5, exhibited a wide variety of phases including disordered, lamellar, cylinders, perforated lamellar, and gyroid, as a function of the sulfonation level in the PSS block. In this range of block ratio, only lamellar phases are expected in conventional block copolymers with no ions present. It was suggested the standard

Scheme 1. Synthetic Scheme for P(VDF-*co*-HFP)-*b*-SPS

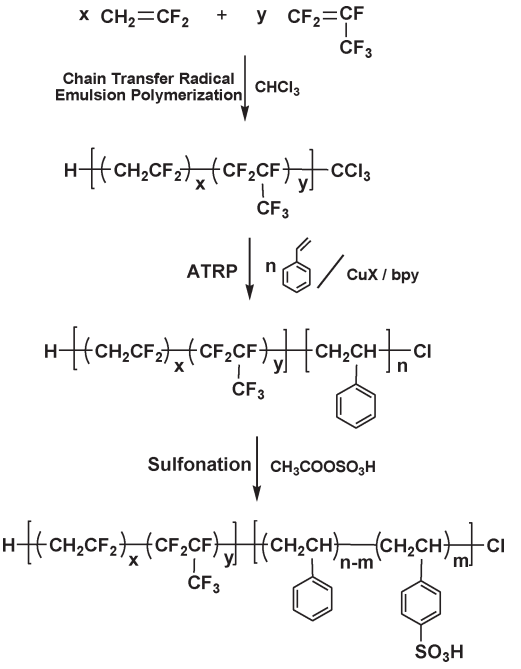

diblock theories are insufficient to accurately describe the phase behavior of ion-containing block copolymers and that more sophisticated models incorporating dipolar and electrostatic interactions are needed for these systems.[45] Very recently, Park and Balsara[46] have investigated the effect of alignment of the proton conducting pathways in PSS-*b*-PMB on proton transport properties. Various processing techniques such as solvent casting, pressing, shearing and electric field alignment were used to obtain membranes with different orientation of the lamellar domains, from which the degree of conductivity anisotropy was found to be consistent with the morphological anisotropy observed.[46] Hillmyer and co-workers[47] have prepared diblock ionomers of poly([norbornenyleneethylstyrene-*r*-styrene]-*b*-styrenesulfonic acid) (PNS-*b*-PSSA) in which the norbornenylene groups were cross-linked by ring-opening metathesis polymerization (ROMP) during membrane casting. A bicontinuous morphology was observed where the PSSA domain size increases directly with the molecular weight of the diblock copolymer; at 90% RH, proton conductivity was found to increase with decreasing PSSA domain size, which is attributed to the capillary condensation effects in smaller ionic domains.[47]

Sulfonated block copolymers possessing fluorinated segments have several advantages including increased thermal and chemical stability, low water absorptivity and higher resistance to oxidation over hydrocarbon analogues. Furthermore, the hydrophobicity of the fluorocarbon block may lead to a higher degree of hydrophilic/hydrophobic microphase separation.[48] Recently, diblock ionomer systems based on sulfonated poly([vinylidene difluoride-*co*-hexafluoropropylene]-*b*-styrene) [P(VDF-*co*-HFP)-*b*-SPS] possessing a hydrophobic fluorous linear segment attached to a hydrophilic sulfonated styrene block have been reported.[49−51] These were prepared by ATRP of styrene from a fluoropolymer macroinitiator, followed by postsulfonation (Scheme 1). This partially fluorinated diblock ionomer system provides great structural control over the lengths of both the fluorinated and the polystyrene segments as well as the ion content via degree of

Scheme 2. P(VDF-*co*-HFP)-*b*-SPS Membranes Studied

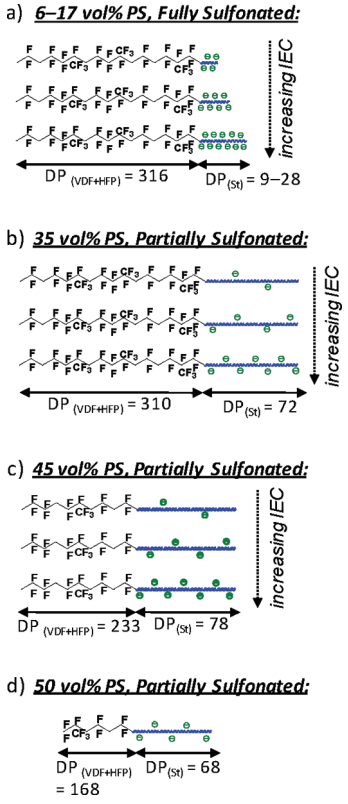

sulfonation of the PS block. The presence of the fluorinated block is reported to improve phase separation, and thereby enhanced proton conductivity compared to random copolymers of styrene and styrenesulfonic acid (PS-*r*-PSSA) as well as to other nonfluorous polystyrene-based block ionomers (i.e., S-SEBS, S-SIBS).[50]

In this paper, we utilize the P(VDF-*co*-HFP)-*b*-SPS diblock ionomer approach to further elucidate structure−property relationships by preparing several series of diblocks possessing different block ratios (Scheme 2). Within each membrane series, the ion content was controlled either by varying the length of the fully sulfonated polystyrene (PS) block (Scheme 2a), or by changing the degree of sulfonation of a fixed PS block (Scheme 2, parts b and c). Proton conductivities, proton mobilities, water content, and acid concentration are studied and compared. As anticipated, the membrane morphology plays a profound role on proton transport but surprisingly, the degree of sulfonation of the PS block plays a stronger role as it determines the extent of ionic purity and connectivity within the so-called "proton-conducting channels". A previous neutron scattering study[52] indicated that the ionic channels in these diblock membranes consist of ionic aggregates of polystyrenesulfonic acid (PSSA) in a matrix of nonsulfonated PS. Thus, here, *ionic purity* is defined as the proportion of ionic PSSA aggregates within the PSSA/PS domains, and is directly related to the degree of sulfonation of the PS segment. The structure−property relationships reported in this work provide useful insights into the design of next-generation proton-conducting membranes.

RESULTS AND DISCUSSION

Synthesis of P(VDF-*co*-HFP)-*b*-SPS Diblock Copolymers. Diblock ionomers of sulfonated poly([vinylidene difluoride-*co*-hexafluoropropylene]-*b*-styrene) [P(VDF-*co*-HFP)-*b*-SPS] were synthesized according to Scheme 1[49,50] Trichloromethyl-terminated fluoropolymers of vinylidene difluoride (VDF) and hexafluoropropylene (HFP) were obtained by emulsion copolymerization in the presence of chloroform as the chain transfer agent. The resulting CCl_3-terminated P(VDF-*co*-CTFE) were subsequently used as macroinitiators in the atom transfer radical polymerization (ATRP) of styrene to yield P(VDF-*co*-HFP)-*b*-PS diblock copolymers. Postsulfonation with acetyl sulfate confered sulfonic acid ($-SO_3H$) groups onto the polystyrene segment. The ionicity, and thus ion exchange capacity (IEC), of the P(VDF-*co*-HFP)-*b*-SPS diblock copolymers were controlled either by varying the length of a fully sulfonated polystyrene block, or by varying the degree of sulfonation on a fixed polystyrene segment. In the former case, the fully sulfonated polystyrene block was kept relatively short compared to the hydrophobic fluorous block in order to yield water-insoluble diblock copolymers.

Gel permeation chromatography (GPC) and NMR spectroscopy were employed to verify each reaction step and to determine the molecular weights of the block segments. GPC traces of the P(VDF-*co*-HFP) macroinitiators and their resulting P(VDF-*co*-HFP)-*b*-PS diblock copolymers were obtained (see Supporting Information, Figure S1). After ATRP, GPC traces shift to a higher molecular weight, indicating the polymerization of styrene onto the macroinitiator. The unimodal GPC peak of the diblock copolymer indicates that the $-CCl_3$ terminus of the fluorous macroinitiator is a single initiator unit, i.e., no double or triple initiation, which is consistent with previous reports on CCl_3-terminated macroinitiators.[53−55]

Figure 1 shows typical ^{1}H NMR spectra of a P(VDF-*co*-HFP) macroinitiator (Figure 1a) and its resulting P(VDF-*co*-HFP)-*b*-PS diblock copolymer (Figure 1b). Peaks at 2.8−3.5 ppm (peak a) correspond to head-to-tail structures of VDF sequences, whereas peaks observed between 2.3−2.6 ppm (peak a′) are due to head-to-head or tail-to-tail structures.[49] These peaks are observed for both the macroinitiator and the resulting diblock copolymer. The presence of the $-CCl_3$ terminal group on the macroinitiator was also confirmed by ^{1}H NMR: the small peaks at 3.7−3.8 ppm (peak i, see inset) are due to CCl_3-related structures of $-C\mathbf{H_2}^*-CF_2-CCl_3$ or $-CF_2-C\mathbf{H_2}^*-CCl_3$; small peaks at 6.2−6.4 ppm (peak j) are due to H-terminated chains with structures of $-CF_2-CH_2-CF_2\mathbf{H}^*$ or $-CH_2-CH_2-CF_2\mathbf{H}^*$. The ratio of integrals of peaks i to j provides an estimation of the ratio of $-CCl_3$ to H-terminated chain ends. This ratio was typically found to be 0.85 ± 0.15, which suggests that one terminal group is not in large excess of the other. The compositions of the P(VDF-*co*-HFP) macroinitiators were determined by ^{19}F NMR spectroscopy (see Supporting Information, Figure S2) as previously described,[56] and found to be 84 ± 3% of VDF and 16 ± 2% of HFP.

As shown in Figure 1b, the ^{1}H NMR spectrum of P(VDF-*co*-HFP)-*b*-PS possesses additional peaks at 1.3−1.7 ppm (peak b, methylene, 2H), 1.8−2.0 ppm (peak c, benzylic, 1H), and 6.4−7.4 ppm (peaks d and e, aryl, 5H), which further indicates the successful polymerization of styrene onto the macroinitiator. Quantitative analysis of the styrene units is obtained by the ratio of integrated signals due to the aromatic styrenic protons (peaks d and e) and the methylene protons of VDF (peaks a and a′), as follows:

$$\frac{\mathrm{St}}{\mathrm{VDF}} = \frac{D + E}{A + A'} \times \frac{2}{5} \quad (1)$$

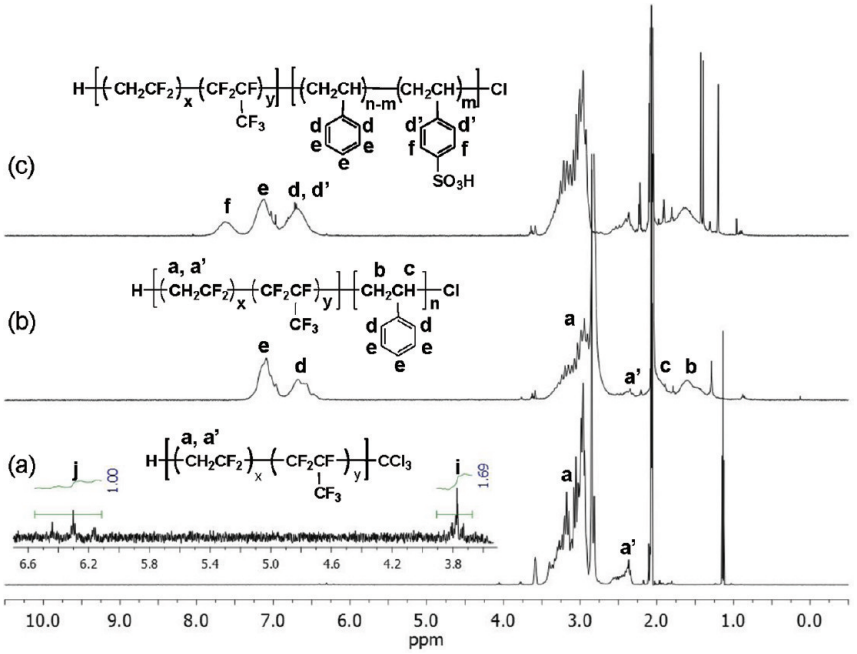

Figure 1. ^{1}H NMR spectra of (a) P(VDF-*co*-HFP) macroinitiator, (b) P(VDF-*co*-HFP)-*b*-PS diblock, and (c) partially sulfonated P(VDF-*co*-HFP)-*b*-SPS (DS = 37%).

Table 1. Chemical Compositions of P(VDF-*co*-HFP)-*b*-PS Parent Diblock Copolymers

	P(VDF-*co*-HFP) macroinitiator		P(VDF-*co*-HFP)-*b*-PS				
diblock copolymer	$M_{n,GPC}$[a] (Da)	$DP_{(VDF+HFP)}$[b]	$M_{n,GPC}$[a] (Da)	$M_{n,NMR}$[d] (Da)	$M_{n,NMR\ (PS)}$[e] (Da)	$DP_{(St)}$[f]	Vol % PS[g]
1	24 300	316	N/A[c]	25 200	900	9	6
2	24 300	316	N/A[c]	25 600	1300	13	8
3	24 300	316	N/A[c]	26 100	1800	17	11
4	24 300	316	N/A[c]	26 400	2100	20	13
5	24 300	316	26 200	27 200	2900	28	17
6	23 900	310	29 900	31 400	7500	72	35
7	17 900	233	25 300	26 000	8100	78	45
8	12 100	168	18 700	19 200	7100	68	50

[a] Measured by THF−GPC, calibrated with linear PS standards. [b] Combined degree of polymerization of VDF and HFP, calculated using $M_{n,GPC}$ [P(VDF-*co*-HFP)] and the mole ratio of VDF/HFP from ^{19}F NMR. [c] Increase in molecular weight could not be measured accurately by GPC. [d] Calculated using $M_{n,GPC}$ [P(VDF-*co*-HFP)] and the ratio of St/VDF from ^{1}H NMR. [e] Molecular weight of the polystyrene segment, calculated from the difference between $M_{n,NMR}$ [P(VDF-*co*-HFP)-*b*-PS] and $M_{n,GPC}$ [P(VDF-*co*-HFP)]. [f] Degree of polymerization of styrene, calculated from $M_{n,NMR}$ [polystyrene]. [g] Volume percentage of polystyrene in the diblock copolymer, calculated according to eq 2.

where D, E, A and A′ are the integrals of peaks d, e, a and a′ in Figure 1b, respectively. The molecular weights of the diblock estimated from NMR were comparable to those estimated using GPC data, as shown in Table 1.

The volumes of the fluorous and the styrenic segments were estimated using their respective pure component density (1.78 g/cm^3 for P(VDF-*co*-HFP), and 1.05 g/cm^3 for polystyrene). The volume percentage of polystyrene (vol % PS) was calculated by:

$$\text{vol \% PS} = \frac{\dfrac{M_{n,\,NMR(PS)}}{\rho_{PS}}}{\dfrac{M_{n,\,NMR(PS)}}{\rho_{PS}} + \dfrac{M_{n,\,GPC(P(VDF-co-HFP)}}{\rho_{P(PVDF-co-HFP)}}} \qquad (2)$$

where $M_{n,NMR\ (PS)}$ and $M_{n,GPC\ (P(VDF\text{-}co\text{-}HFP))}$ are the number-average molecular weights of the polystyrene and the fluorous segments, respectively; ρ_{PS} and $\rho_{P(VDF\text{-}co\text{-}HFP)}$ are their respective densities. The estimated volume percentages of polystyrene in the diblock copolymers are also listed in Table 1. The volume percentages based on sulfonated polystyrene were also considered (see Supporting Information, Table S1): using space-filling model software,[57] it was estimated that addition of a $-SO_3H$ group would increase the volume of a *single* styrene unit by ∼30%. For the P(VDF-*co*-HFP)-*b*-PS diblock copolymers, complete sulfonation of the polystyrene blocks was estimated to increase the volume percentages of the polystyrene portion of the entire diblock by 2−4 vol %. In the case of partial sulfonation of the polystyrene blocks, sulfonation increases the volume percentages by only 2−3 vol %. Thus, changes in nonfluorous volume fraction due to the incorporation of $-SO_3H$ groups is very small, and can be neglected.

dx.doi.org/10.1021/ma2010469 |*Macromolecules* 2011, 44, 8845–8857

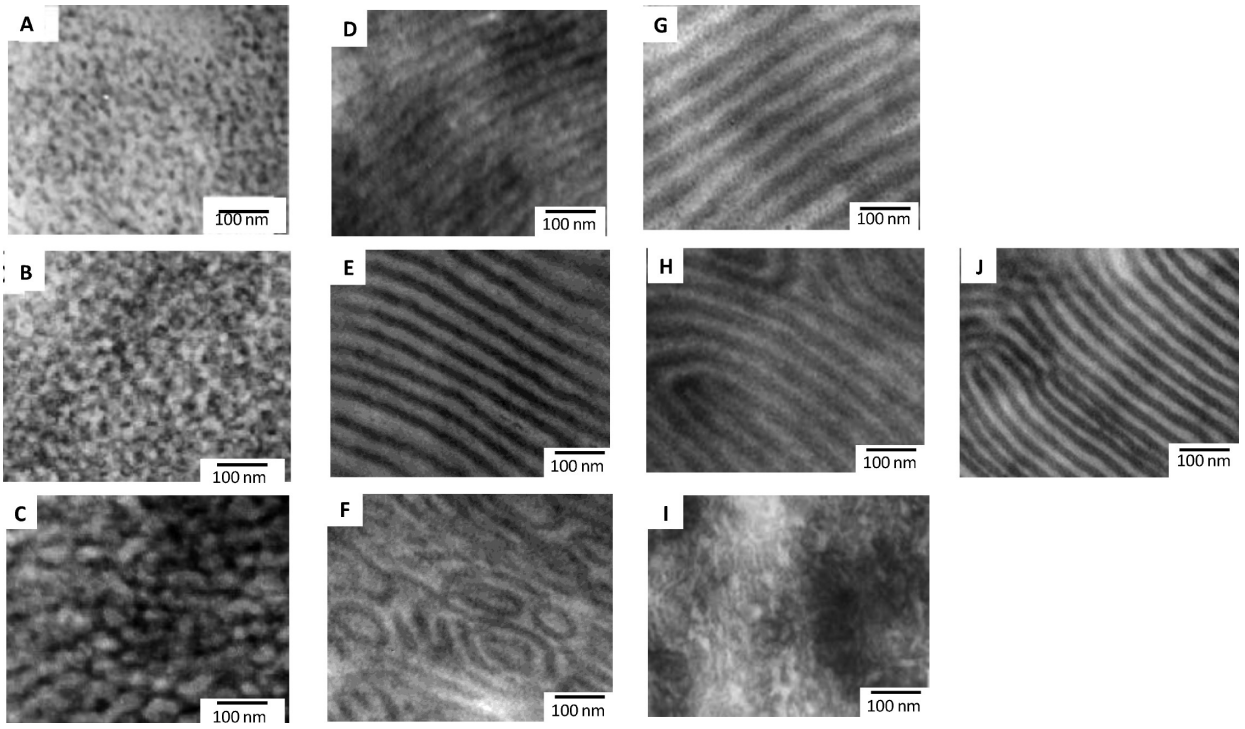

Figure 2. TEM images of selected P(VDF-*co*-HFP)-*b*-SPS membranes from the 6−17 vol % PS series with IECs (mmol/g) of (A) 0.46, (B) 0.70, (C) 1.20; the 35 vol % PS series with IECs of (D) 0.42, (E) 0.68, (F) 0.73; the 45 vol % PS series with IECs of (G) 0.62, (H) 0.89, (I) 1.31; and the 50 vol % PS series with an IEC of (J) 1.09.

P(VDF-*co*-HFP)-*b*-PS diblock copolymers possessing 6, 8, 11, 13, 17, 35, 45, and 50 vol % PS were systematically prepared, and their compositions are described in Table 1. For parent diblocks with low PS content (6−17 vol %), the polystyrene segments were *fully* sulfonated. Collectively, these yield a series of proton-conducting membranes in which the ionic content is controlled by varying the length of the fully sulfonated polystyrene, as illustrated in Scheme 2a. Whereas for parent diblocks with higher polystyrene content (35, 45, and 50 vol % PS), complete sulfonation of the polystyrene segments leads to water-soluble polymers; thus, the parent diblocks were *partially* sulfonated to provide membranes with different ionicity, as illustrated in Scheme 2, parts b and c. In these membranes series, IEC was controlled by varying the degree of sulfonation on a fixed polystyrene block length. The 50 vol % PS diblock possessed a relatively short fluorous segment ($DP_{(VDF+HFP)}$ = 168) compared to the 35 and 45 vol % PS diblocks ($DP_{(VDF+HFP)}$ ~ 250−300) in order to yield a high PS content diblock. Only one IEC sample is reported for the 50 vol % PS diblock (Scheme 2d).

A typical ^{1}H NMR spectrum of a partially sulfonated diblock copolymer is given in Figure 2c. The peak at 6.8−7.4 ppm (peak e) is due to *m*- and *p*- protons on the nonsulfonated styrene units; whereas the peak at 7.4 to 7.8 ppm (peak f) is assigned to aromatic protons adjacent to the sulfonate group. The degree of sulfonation (DS, %) is estimated using the ratio of integrals for peaks e and f, as follows:

$$\mathrm{DS}\ (\%) = \frac{\frac{F}{2}}{\frac{F}{2} + \frac{E}{3}} \times 100\% \qquad (3)$$

where *E* and *F* represent the integrals of peaks e and f in Figure 2c, respectively.

The chemical compositions, degrees of sulfonation and IECs for the P(VDF-*co*-HFP)-*b*-SPS membranes are summarized in Table 2. For ease of discussion, the membranes series are referred to their PS content: 6−17, 35, 45, and 50 vol % PS, and to the degree of sulfonation: *fully* or *partially* sulfonated.

TEM. The nanostructure and morphology of the membranes were investigated using transmission electron microscopy (TEM) on cross-sectional slices (~100 nm) of dry membranes. Membranes were stained with lead acetate prior to imaging, therefore the dark areas in the TEMs correspond to regions of high ionic content. TEM images of selected membranes from the 6−17 vol % PS, fully sulfonated series are shown in Figure 2, parts A, B, and C. No ion phase separation morphology is observed for the membrane possessing the lowest IEC of 0.07 mmol/g (not shown). With increasing IEC (>0.40 mmol/g), a phase-separated morphology characterized by disordered ionic clusters is observed (Figure 2, parts A, B, and C). The size of the ion clusters (dark domains) is found to increase from 6 to 20 nm as IEC increases from 0.40 to 1.13 mmol/g, and is attributed to the increasing length of the fully sulfonated polystyrene segment, which leads to enhanced phase separation and aggregation of larger ionic cluster. Similar trends in ionic domain size have been previously reported by our group.[58,59] Using graft copolymers comprising polystyrene main chain and ionic polystyrenesulfonic acid graft chains (PS-*g*-PSSA), it is reported[59] that ionic cluster size and the degree of phase separation increase as the length of the PSSA graft chains increase.

In general, ordered lamellar-like morphologies are observed in partially sulfonated membranes, with low to intermediate IEC, for the 35 (Figure 2D,E), 45 (Figure 2G,H), and 50 vol % (Figure 2J) PS series, and are consistent with the morphological phase diagram reported for diblock copolymers of poly(styrene-*b*-isoprene), in

Table 2. Chemical Compositions of P(VDF-*co*-HFP)-*b*-SPS Membranes

series	membrane	$M_{n\ (fluorous)}$[a] (Da)	$M_{n\ (PS)}$[b] (Da)	DS[c] (%)	IEC[d] (mmol/g)
6−17 vol % PS, fully sulfonated	1−1	24 300	900	100	0.34 ± 0.02
	1−2		1300		0.46 ± 0.01
	1−3		1800		0.64 ± 0.02
	1−4		2100		0.70 ± 0.04
	1−5		2900		1.20 ± 0.03
35 vol % PS, partially sulfonated	2−1	23 900	7500	16	0.31 ± 0.02
	2−2			21	0.42 ± 0.01
	2−3			27	0.52 ± 0.02
	2−4			32	0.59 ± 0.02
	2−5			37	0.68 ± 0.02
	2−6			41	0.73 ± 0.03
45 vol % PS, partially sulfonated	3−1	17 900	8100	12	0.26 ± 0.01
	3−2			17	0.53 ± 0.02
	3−3			22	0.72 ± 0.05
	3−4			32	0.89 ± 0.03
	3−5			40	1.18 ± 0.05
	3−6			49	1.31 ± 0.05
50 vol % PS, partially sulfonated	4−1	12 100	7100	35	1.09 ± 0.05

[a] Molecular weight of the fluorous segment, measured by THF-GPC using linear PS standards. [b] Molecular weight of the polystyrene segment, estimated using the ratio of St/VDF from ^{1}H NMR. [c] On the basis of ^{1}H NMR according to eq 3. [d] Measured by acid−base titration.

which pure lamellar structures have been observed for 35 to 65 vol % PS block fractions.[60,61] In the present work, clear signs of phase separation are observed for the 35 vol % PS series even for the lowest IEC sample (0.31 mmol/g, not shown). As IEC increases (from 0.42 to 0.68 mmol/g, Figure 2D,E), phase separation becomes more distinct, and the interface, sharper. The width of the ionic lamellae is ∼15−20 nm, and the interdomain spacing is ∼20−40 nm. For higher IEC membranes (e.g., 0.73 mmol/g, Figure 2F), the morphology becomes disordered. Such an order−disorder transition may have a significant impact on the membrane properties, as will be discussed later. Changes in morphology with sulfonation have been reported in other sulfonated block copolymer systems. For instance, using sulfonated poly(styrene-*b*-isobutylene-*b*-styrene) triblock copolymers (31 wt % PS), Elabd et al.[40] observed a morphological transition from cylinders to lamellar at DS of 13%, and a second periodic to nonperiodic cocontinuous morphology at DS > 40%. Park and Balsara[45] reported that sulfonated poly(styrene-*b*-methylbutylene) (PS volume fraction of 0.45−0.5) displayed a range of phases including disordered, lamellar, cylindrical, and gyroid as a function of sulfonation in the styrene block. The work of Mauritz et al.[35] on sulfonated poly(styrene-*b*-[ethylene-*r*-butylene]-*b*-styrene) revealed morphological transitions from hexagonally packed cylinders to lamellae as the DS increases from 0 to 12%. A few mechanisms have been suggested for the morphological shift with sulfonation. These include changes in chain conformation of the sulfonated block due to strong dipole and electrostatic interactions between ionic monomers, increased Flory−Huggins interaction parameter (χ) between the sulfonated and unsulfonated segments, and increased interfacial surface tension between phases leading to a minimization of interfacial surface area.[35,45,62]

TEM micrographs of partially sulfonated membranes for the 45 vol % PS series with IECs of 0.62 and 0.89 mmol/g are shown in Figure 2, parts G and H, respectively. The width of the ionic lamellae phase is found to be 20−30 nm, i.e., larger than the 35 vol % PS membranes; but possessing a interdomain spacing of 20−40 nm, which is similar to the 35 vol % PS membranes. A disordered morphology is observed for high IEC membranes (1.31 mmol/g, Figure 2I). For the 50 vol % PS membrane possessing an IEC of 1.09 mmol/g (Figure 2J), the width of the ionic lamellae is found to be 15−20 nm with a fluorocarbon interdomain spacing of 10−25 nm. The fluorocarbon and ionic domains are narrower compared to the 35 vol % and 45 vol % PS membranes, due to both the shorter fluorous and ionic segments in the 50 vol % PS membrane.

Although the TEM images shown above are for dry membranes, the morphology is expected to be preserved in the water-swollen membranes, as evidenced in our previous study.[52] Small-angle neutron scattering (SANS) analysis of P(VDF-*co*-HFP)-*b*-SPS membranes showed that, upon hydration, the overall morphology of the membranes is maintained, but the dimensions of lamellar spacing vary accordingly.[52]

Water Sorption. The water sorption properties of the membranes in the protonic form are expressed both as water content and molar ratio of water to sulfonic acid ($[H_2O]/[SO_3^-]$, λ). Water content and λ versus IEC are plotted in Figure 3 (that for Nafion 117, IEC = 0.91 mmol/g, is also plotted for comparison). As expected, water sorption increases with IEC for all membrane series.

Considerable differences are found in water sorption behavior between different series of membranes. In the low IEC range (<0.6 mmol/g), the partially sulfonated membranes absorb significantly less water than the fully sulfonated membranes. For instance, for an IEC range of 0.3 to 0.6 mmol/g, water contents are found to be 2−12 and 5−21 wt % for the partially sulfonated membranes with 35 and 45 vol % PS, respectively; whereas the water content is 19−27 wt % for the fully sulfonated membranes with 6−17 vol % PS. The lower water uptake in the former is attributed to the PS segment being only partially sulfonated. A neutron scattering study[52] on partially sulfonated P(VDF-*co*-HFP)-*b*-SPS membranes reveals a hierarchical membrane

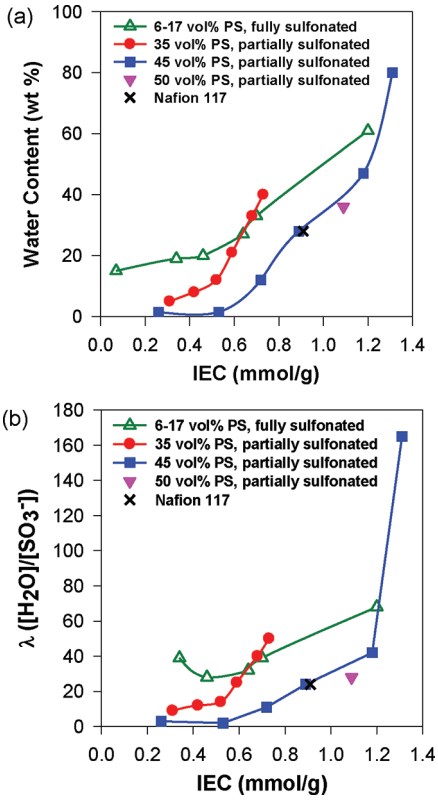

Figure 3. (a) Water content vs IEC; (b) λ vs IEC for P(VDF-*co*-HFP)-*b*-SPS membranes with 6−17 (green △), 35 (red ●), 45 (blue ■) and 50 (purple ▼) vol % polystyrene. Note: open symbols represent fully sulfonated membranes; filled symbols, partially sulfonated.

microstructure, involving two levels of phase separation, as illustrated in Figure 4. At one level of phase separation (Figure 4a), the hydrophobic fluoropolymer segment segregates from the sulfonated PS segment forming alternating fluorocarbon and ionic PSSA/PS domains; and within the ionic PSSA/PS domain (Figure 4b), a sublevel of phase separation exists in which ionic aggregates/clusters of PSSA are formed in a matrix of the PS host, similar to that found in randomly sulfonated polystyrene (PS-*r*-PSSA).[24,63,64] In addition to the hydrophobic fluorocarbon domains, the nonsulfonated PS matrix provides further opposition to water swelling. In contrast, for the 6−17 vol % PS membranes, the PS segments are fully sulfonated and swell considerably even for low IEC membranes.

As IEC is increased above 0.6 mmol/g, the water sorption of all the membrane series are observed to increase significantly (Figure 3). For the partially sulfonated, 35 and 45 vol % PS membranes, water sorption shows a slower rate of increase with IEC initially, followed by a sharp increase, indicative of reaching an interconnected network of PSSA clusters within the ionic PSSA/PS domains, as depicted in Figure 4b: For low ion contents, or low degrees of sulfonation (Figure 4b left), the ionic purity within the PSSA/PS domains is low—i.e., the PSSA/PS domains contain mostly of the nonsulfonated PS host matrix. Both the number and the size of the ionic PSSA clusters are small and they remain relatively isolated and thus, water uptake is low. With increasing degrees of sulfonation (Figure 4b right), the ionic purity and the cluster size increase, leading to increasing amounts of water absorbed; eventually, an interconnected network of ionic PSSA clusters is formed for which water uptake increases dramatically.

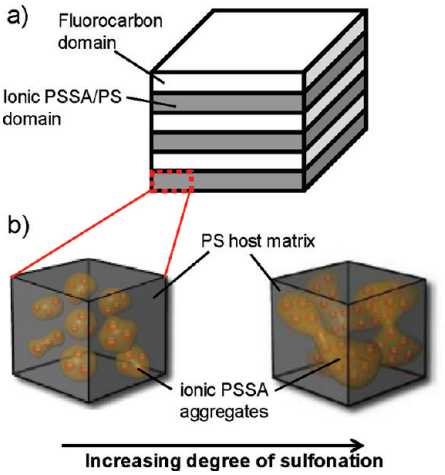

Figure 4. Schematic representation of the hierarchical microstructure in P(VDF-*co*-HFP)-*b*-SPS: (a) the large scale morphology consists of stacks of alternating fluorocarbon and ionic PSSA/PS domains; (b) within the PSSA/PS domains, ionic aggregates of PSSA exist in a matrix of host PS.

Despite the fully sulfonated 6−17 vol % PS membranes exhibiting relatively large water sorption at low IEC ranges, they do not exhibit a threshold effect and water swelling is less sensitive to changes in IEC. This may be attributed to the formation of smaller short-range ionic domains (Figure 2, parts A, B, and C), which allows for a greater continuity in the hydrophobic fluorocarbon matrix that resists osmotic pressure-driven swelling at the high IEC ranges.

Comparisons between the different series of partially sulfonated membranes reveal that water sorption decreases with increasing PS content in the membranes. For instance, over the IEC range, 0.5−0.7 mmol/g, the water content is 12−33 and 2−12 wt % for 35 and 45 vol % PS membranes, respectively; and for IEC of ~1.1 mmol/g, the water content is 47 and 36 wt % for the 45 and 50 vol % PS membranes, respectively. That is, for a given IEC, water content decreases in the order of 35 > 45 > 50 vol % PS. To achieve an IEC of ~0.7 mmol/g, the 35 vol % PS polymer membrane requires a degree of sulfonation (DS) of ~40%; whereas the 45 vol % PS membrane requires only ~20% DS (Table 2). The higher degree of sulfonation reduces the proportion of nonsulfonated PS and allows for closer spatial proximity between neighboring sulfonic acid groups, which may lead to the formation of larger and more interconnected PSSA clusters. Membranes with high PS content require relatively low degrees of sulfonation to obtain a given IEC value; thus, the ionic purity within the ionic PSSA/PS domains is low, which restricts the formation of an interconnected ionic cluster network. Simply put, high PS content membranes are less prone to water swelling, which significantly impacts proton transport within them.

Proton Conductivity. *In plane* proton conductivities versus IEC for various membrane series are plotted in Figure 5a. For the 35 and 45 vol % PS membranes, conductivities increase initially with IEC, and decrease upon further increases. Figure 6a plots the acid concentration ($[-SO_3H]$) in hydrated membranes. For the partially sulfonated 35 and 45 vol % PS membranes, the $[-SO_3H]$ initially increases with IEC but dilution occurs with further increases. These trends are consistent with the water sorption behavior, as shown in Figure 3a: For the 35 and 45 vol % PS membranes, water sorption increases sharply above IEC values

dx.doi.org/10.1021/ma2010469 |*Macromolecules* 2011, 44, 8845–8857

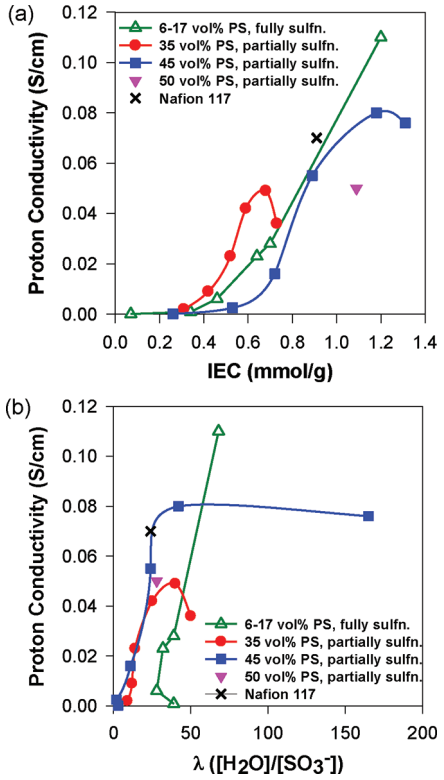

Figure 5. (a) Proton conductivity vs IEC and (b) proton conductivity vs λ for P(VDF-*co*-HFP)-*b*-SPS membranes with 6−17 (green △), 35 (red ●), 45 (blue ■), and 50 (purple ▼) vol % polystyrene. Note: open symbols represent fully sulfonated membranes; filled symbols, partially sulfonated.

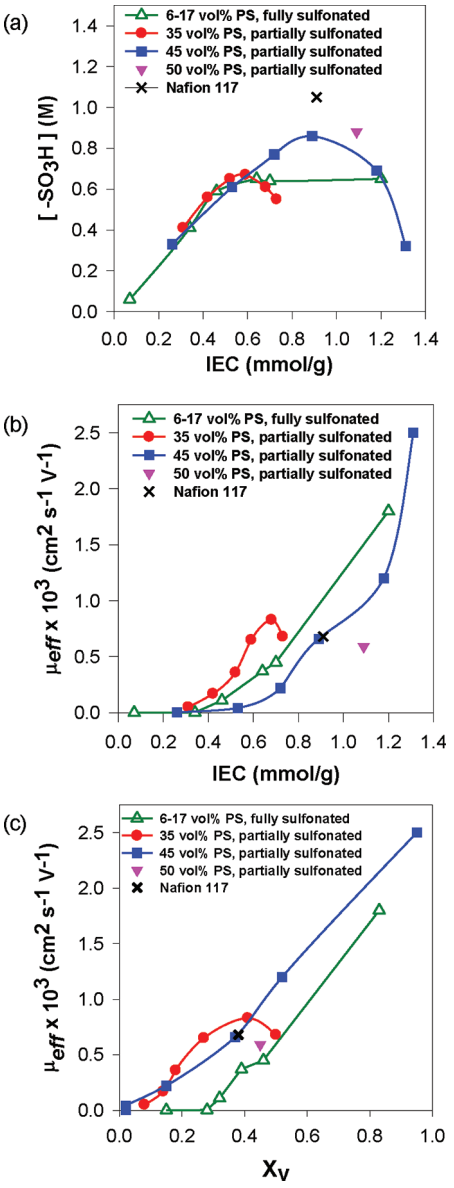

Figure 6. (a) [$-SO_3H$] in hydrated membranes vs IEC, (b) *effective* proton mobility (μ_{eff}) vs IEC, and (c) μ_{eff} vs water volume fraction (X_v) for P(VDF-*co*-HFP)-*b*-SPS membranes with 6−17 (green △), 35 (red ●), 45 (blue ■), and 50 (purple ▼) vol % polystyrene. Note: open symbols represent fully sulfonated membranes; filled symbols, partially sulfonated.

of 0.5 and 0.7 mmol/g, respectively. Thus, the drop in proton conductivity observed for high IEC membranes is due to acid dilution caused by excessive water uptake, as reported for other sulfonated polystyrene-based copolymer systems.[27,37,42,58,65,66]

The fully sulfonated, 6−17 vol % PS membranes exhibit a continuous increase in proton conductivity over the range of IEC studied (Figure 5a), and possess a proton conductivity of 0.11 S cm^{-1} at an IEC of 1.20 mmol/g − the highest value observed in this study. Water sorption in the 6−17 vol % PS membranes is relatively less sensitive to changes in IEC compared to the other membrane series (Figures 3a and b), which enables these membranes to maintain a reasonably high [$-SO_3H$], which remains constant at ∼0.6 M for IECs > 0.4 mmol/g.

Comparisons between partially sulfonated membranes with different PS contents reveal that membranes with lower PS content possess a lower IEC threshold beyond which conductivity increases sharply with IEC (Figure 5a). For the 35 and 45 vol % PS membrane series, the threshold is ∼0.4 and ∼0.7 mmol/g, respectively. Over a similar IEC range of 0.3 to 0.7 mmol/g, the 35 vol % PS membranes exhibit higher proton conductivities than the 45 vol % PS membranes. A lower IEC threshold and greater proton conductivity in the 35 vol % PS membranes are due to the relatively higher degree of sulfonation. As discussed previously, a higher degree of sulfonation results in closer spatial proximity between neighboring sulfonic acid groups, which in turn, leads to the formation of larger ionic PSSA clusters and a more interconnected ionic network. This allows for higher water sorption as well as enhanced proton transport with the hydrophilic PSSA/PS domains.

It is reported that perfluorosulfonic acid ionomer membranes show a significant increase in proton conductivity when $\lambda > 6$.[67] Figure 5b shows the relationship between proton conductivity as a function of water content (λ). For λ values of 10−20, the partially sulfonated, 35 and 45 vol % PS membranes exhibit similar proton conductivities. However, for λ values between 20 and 40, the ordering of conductivity is 45 > 35 > 6−17 vol % PS. The maximum proton conductivity value occurs when λ ∼40 for both the 35 and 45 vol % PS membranes, and conductivity drops with further increases in λ (>40). Similar observations are reported in other proton conducting block copolymer systems.[68] It is concluded that for sulfonated block copolymer membranes, increasing λ values from 0 to 40 increases the proton conductivity by enhancing proton mobility; however, beyond this, further

dx.doi.org/10.1021/ma2010469 |*Macromolecules* 2011, 44, 8845–8857

Table 3. In-Plane and Through-Plane Conductivity of Selected P(VDF-*co*-HFP)-*b*-SPS Membranes

membrane	IEC (mmol/g)	X_v	σ_x (S cm^{-1})	σ_y (S cm^{-1})	σ_z (S cm^{-1})	$\sigma_{\parallel/\perp}$[a]
6−17 vol % PS, fully sulfonated	0.64	0.39	0.025 ± 0.002	0.021 ± 0.002	0.030 ± 0.004	0.8
35 vol % PS, partially sulfonated	0.68	0.41	0.049 ± 0.002	0.047 ± 0.001	0.016 ± 0.002	3.0
45 vol % PS, partially sulfonated	0.89	0.37	0.054 ± 0.002	0.056 ± 0.001	0.022 ± 0.001	2.5
50 vol % PS, partially sulfonated	1.09	0.45	0.047 ± 0.002	0.048 ± 0.002	0.017 ± 0.003	2.8
Nafion 117	0.91	0.38	0.077 ± 0.001	0.075 ± 0.002	0.069 ± 0.002	1.1

[a] Expressed as the ratio of in-plane ($\sigma_\parallel$) to through-plane ($\sigma_\perp$) conductivity. $\sigma_\parallel$ is obtained from the average of σ_x and σ_y.

increases in λ dilute the acid concentration and this effect outweighs any further increase in proton mobility. Such acid dilution does not occur in the fully sulfonated 6−17 vol % PS membranes due to their limited water swelling at high IEC, and thus these membranes exhibit a continuous increase in proton conductivity even beyond λ values of 40.

Proton Mobility. The *effective* proton mobility, μ_{eff}—where the effects of acid concentration on conductivity are removed—provides meaningful insights into the combined factors of degree of acid dissociation, ionic channel tortuosity, and spatial proximity between neighboring acid groups within the ionic domains.[68] Figure 6b shows the relationship between μ_{eff} and IEC for the various series of membranes. μ_{eff} generally increases with IEC in these membranes, which is expected, as increasing the IEC leads to increased water sorption and proton mobility. Comparisons between the various partially sulfonated membranes indicate that proton mobility is higher for membranes with lower PS content. For instance, for IEC values between 0.4 and 0.7 mmol/g, μ_{eff} is $(0.17-0.83) \times 10^{-3}$ cm^2 s^{-1} V^{-1} for the 35 vol % PS membranes compared to $(0.04-0.22) \times 10^{-3}$ cm^2 s^{-1} V^{-1} for the 45 vol % PS membranes. The greater proton mobility in the 35 vol % PS membranes is attributed to the relatively higher degree of sulfonation and therefore, closer spatial proximity between acid groups. For example, to obtain an IEC of ∼0.7 mmol/g, for the 35 vol % PS membranes, a degree of sulfonation of ∼40% is required; whereas ∼20% is required for the 45 vol % PS membranes (Table 2). At this IEC, in the 35 vol % PS membranes, each sulfonic acid group is separated by 1 to 2 unsulfonated styrene units; whereas for the 45 vol % PS membranes, each sulfonic acid is 5 styrene units apart. The high degree of sulfonation favors the formation of larger ionic clusters with greater water sorption, which promotes proton dissociation and transport within the ionic channels. It is worth noting that the 35 vol % PS membrane with the highest IEC exhibits a lower proton mobility. This might be explained from the TEM image (Figure 2F), which shows disordered and tortuous ionic channels.

Plots of μ_{eff} versus water volume fraction (X_v) (Figure 6c) can be used to gain insights into the degree of tortuosity and connectivity of the ionic domains. The partially sulfonated 35, 45, and 50 vol % PS membranes possess significantly greater μ_{eff} than the fully sulfonated 6−17 vol % PS membranes. This suggests that the ionic channels in the partially sulfonated membranes are more contiguous with fewer dead ends, which is consistent with the morphology revealed in the TEM images (Figure 2D−J). In contrast, the fully sulfonated membranes are characterized as possessing highly encumbered ionic pathways.

Conductivity Anisotropy. In an operating PEMFC, proton transport is perpendicular to the plane of the membrane—in the *through-plane* direction; thus, anisotropies in both membrane morphology and proton conductivity are important factors for evaluating PEM materials. Soboleva et al.[69] report that the degree of conductivity anisotropy in Nafion is influenced by the casting method: extruded membranes (Nafion 112, 1135, 115, and 117) demonstrate relatively anisotropic conductivity, whereas solution-cast membranes (Nafion 211) exhibit isotropic conductivity; Gebel et al.[70] reported on the anisotropic proton conductivity in sulfonated polyimide membranes possessing distinct morphological anisotropy. Park and Balsara[46] have recently studied conductivity anisotropy in sulfonated poly(styrene-*b*-methylbutylene) membranes possessing controlled orientations of the ionic domains that are obtained from various processing techniques.

In order to examine conductivity anisotropy, proton conductivity in the *in-plane* (both *X* and *Y*) and *through-plane* (*Z*) directions were measured on selected membranes. Membranes possessing similar water volume fractions of ∼0.40 were chosen, that is, IECs of 0.64, 0.68, 0.89, and 1.09 mmol/g for the 6−17, 35, 45, and 50 vol % PS membranes, respectively. Conductivity anisotropy ($\sigma_{\parallel/\perp}$), quantified by the ratio of in-plane ($\sigma_\parallel$) over through-plane ($\sigma_\perp$) conductivity, are given in Table 3. The fully sulfonated 6−17 vol % PS membrane is found to show very similar in-plane and through-plane proton conductivity indicating little anisotropy ($\sigma_{\parallel/\perp}$ = 0.8), which is consistent with the randomly distributed ionic cluster morphology, as revealed by TEM (Figure 2A−C).

For the 35, 45, and 50 vol % PS membranes, the in-plane proton conductivity is found to be greater than the through-plane conductivity, indicating a higher degree of anisotropy, and the hydrophilic proton-conducting domains are oriented along the plane of the membrane in such a way that the alternating hydrophilic and hydrophobic layers are stacked parallel to the membranès surface. This is consistent with the visualized lamellar morphology observed in the TEM analysis (Figure 2D−J). The conductivity anisotropy of Nafion-112 membranes is found to be 1.2, which is in close agreement to previous reports.[69]

CONCLUSION

Diblock ionomers of sulfonated poly([vinylidene difluoride-*co*-hexafluoropropylene]-*b*-styrene) [P(VDF-*co*-HFP)-*b*-SPS], possessing different polystyrene (PS) content, are useful for investigating the role of sulfonation degree and morphology on PEM membrane properties. Membranes with distinct phase-separated morphology were obtained. Membrane properties such as water sorption, acid concentration, proton conductivity and mobility were greatly influenced by the membranes' morphology, visualized by TEM, but moreover by the constituent polymer's degree of sulfonation and the resulting ionic purity within the proton-conducting domains.

Fully sulfonated membranes with 6−17 vol % PS possess disordered ionic clusters for which the cluster size increases with the length of the fully sulfonated styrene segment. Although these fully sulfonated membranes exhibit high water sorption at

low IEC, the water sorption is less sensitive to changes in IEC. Consequently, these membranes are able to possess a high acid concentration, leading to a continuous increase in proton conductivity over a large IEC range. In contrast, partially sulfonated membranes with 35, 45, and 50 vol % PS are characterized by a phase-separated morphology comprising of lamellar structures. At low IEC ranges, these membranes exhibited lower water sorption compared to the fully sulfonated, 6−17 vol % PS membranes, which is attributed to the presence of the hydrophobic PS host matrix that surrounds the ionic PSSA clusters. For partially sulfonated membranes, increasing the PS content of the diblock leads to a lower water uptake and a higher IEC threshold for proton conduction. This is ascribed to the lower degree of sulfonation required, which in turn leads to smaller and more isolated ionic PSSA clusters. Acid dilution effects are more pronounced for the partially sulfonated membranes due to their excessive water uptake at high ion content, resulting in drops in proton conductivity for high IEC membranes. Once an interconnected network of ionic PSSA clusters is formed within the PSSA/PS domains, the lamellar structure of the diblock provides little resistance to swelling. For a similar water volume fraction, proton mobility is observed to be greater in the partially sulfonated membranes due to the presence of long-range, linear ionic domains but conductivity anisotropy is larger. In summary, this work stresses the point that the degree of sulfonation plays a significant role on proton transport as it determines the ionic purity and the connectivity of ionic clusters within a proton-conducting channel.

EXPERIMENTAL SECTION

Materials. Vinylidene difluoride (VDF, SynQuest Laboratory Inc., 99+%), hexafluoropropylene (HFP, Aldrich, 99+%), potassium persulfate (KPS, Allied Chemical, reagent grade), sodium metabisulfite ($Na_2S_2O_5$, Anachemia, anhydrous, reagent grade), chloroform (Caledon, spectrograde), pentadecafluorooctanoic acid (Aldrich, 96%), copper(I) chloride (CuCl, Aldrich, 99.995+%), 2,2′-dipyridyl (bpy, Aldrich, 99+%), 1, 2-dichloroethane (DCE, Caledon, reagent grade), sulfuric acid (Anachemia, 95−98%, ACS reagent), and acetic anhydride (Caledon, reagent grade) were used as received. *n*-Butyl acetate (Caledon, reagent grade) was refluxed with small portions of $KMnO_4$, distilled in the presence of CaH_2 under reduced pressure, and stored under N_2 at −20 °C. Styrene (St, Aldrich, 99+%) was washed twice with aqueous 5% NaOH and twice with water, dried overnight with $MgSO_4$, distilled in the presence of CaH_2 at 40 °C under reduced pressure, and stored under nitrogen at −20 °C. As received Nafion 117 (Du Pont) membranes were pretreated by boiling sequentially in 3% H_2O_2 (by volume), 0.5 M H_2SO_4, and Milli-Q water (18 MΩ, Millipore Systems) for 2 h and stored in Milli-Q water prior to use.

Poly([vinylidene difluoride-*co*-hexafluoropropylene]-*b*-styrene) was synthesized by atom transfer radical polymerization (ATRP) of styrene initiated by a trichloromethyl-terminated fluorous macroinitiator, as previously described.[49,50] The fluorous macroinitiator was prepared by emulsion copolymerization of VDF and HFP in the presence of chloroform, which served as a chain transfer agent. A typical emulsion polymerization was performed as follows: to a 160 mL pressure vessel (Parr Instruments) equipped with a 600 psi pressure relief valve and a magnetic stir bar, an aqueous solution containing water (100 mL), KPS (0.80 g), $Na_2S_2O_5$ (0.58 g), pentadecafluorooctanoic acid (0.04 g), and a predetermined amount of chloroform was added. An initial monomer mixture of 45 mol % HFP and 55 mol % VDF was introduced into the reactor. A constant pressure of 300 psi was maintained by supplying to the vessel a supplemental monomer mixture of 20 mol % HFP and 80 mol % VDF. The polymerization times were varied from 2 to 4 h depending on the amount of chain transfer agent. The resulting P(VDF-*co*-HFP) polymer latex was coagulated by freezing, and then washed repeatedly with water and ethanol. The crude P(VDF-*co*-HFP) macroinitiator was purified by dissolution in acetone and precipitation in ethanol, and then dried at 50 °C under vacuum for 24 h. ^{1}H NMR (500 MHz, acetone-d_6), δ (ppm): 2.8 to 3.5 ($-CF_2-CH_2-CF_2-C\mathbf{H_2}^*-CF_2-CH_2-$), 2.3 to 2.6 ($-CH_2-CF_2-CF_2-C\mathbf{H_2}^*-CH_2-CF_2-$). ^{19}F NMR (400 MHz, acetone-d_6), δ (ppm): −71.4 ($-CH_2-CF_2-CF(\mathbf{CF_3}^*)-CF_2-CH_2$), −76.0 ($-CF_2-CF_2-CF(\mathbf{CF_3}^*)-CH_2-CF_2$), −92.0 to −94.5 ($-CF_2-CH_2-C\mathbf{F_2}^*-CH_2-CF_2$), −96.2 ($-CF_2-CH_2-C\mathbf{F_2}^*-CH_2-CH_2$), −104.4 ($-CF_2-CH_2-C\mathbf{F_2}^*-CF_2-CF(CF_3)-$), −109.7 to −114.5 ($-CH_2-CF_2-C\mathbf{F_2}^*-CH_2-CH_2$), −115.5 to −120.0 ($-CH_2-CF_2-C\mathbf{F_2}^*-CF(CF_3)-CH_2$), −185.1 ($-CF_2-C\mathbf{F}^*(CF_3)-CF_2-$ or $-CH_2-C\mathbf{F}^*(CF_3)-CF_2-$). The composition of the P(VDF-*co*-HFP) macroinitiator was estimated by ^{19}F NMR according to published methods[56] and found to be 16 ± 2 mol % HFP and 84 ± 2 mol % VDF.

Trichloromethyl-terminated P(VDF-*co*-HFP) was subsequently used as a macroinitiator in the ATRP of styrene. Typical procedures for ATRP reactions were as follows: P(VDF-*co*-HFP) macroinitiator (0.50 g), copper(I) chloride (CuCl) (0.064 g), dipyridyl (bpy) (0.30 g) and styrene (1.0 mL) were dissolved in *n*-butyl acetate (3.0 mL) in a dried flask equipped with a rubber septum and a magnetic stir bar. After deoxygenation using three cycles of freeze−pump−thaw, the reaction mixture was heated to 110 °C under a nitrogen blanket for 24 h. The resulting P(VDF-*co*-HFP)-*b*-PS diblock copolymer was purified by dissolving in THF, passing through a column of alumina, precipitating in ethanol and then drying at 50 °C under vacuum for 24 h. ^{1}H NMR (500 MHz, acetone-d_6) δ (ppm): 6.4−7.4 (aryl), 2.8 to 3.5 (methylene, head-to-tail VDF sequences), 2.3 to 2.6 (methylene, head-to-head or tail-to-tail VDF sequence), 1.8 to 2.0 (benzylic), 1.3 to 1.7 (methylene, styrene).

Sulfonation of P(VDF-*co*-HFP)-*b*-PS was carried out in 1,2-dichloroethane according to a procedure reported in the literature,[22] except a reaction temperature of 40 °C was used. A typical sulfonation reaction is as follows: P(VDF-*co*-HFP)-*b*-PS (0.6 g) and 1,2-dichloroethane (15 mL) were added to a 50 mL three-neck flask equipped with a dropping funnel and condenser. The mixture was heated to 50 °C under nitrogen and stirred until complete dissolution. Acetyl sulfate was prepared by injecting acetic anhydride (1.8 mL) and 1,2-dichloroethane (3.0 mL) into a nitrogen-purged vial. The solution was cooled to ∼0 °C in a 10 wt % $CaCl_2$ ice bath after which 95−97% sulfuric acid (0.6 mL) was injected. The resultant acetyl sulfate was immediately added to the polymer solution at 40 °C. Samples sulfonated to various extents were periodically extracted and precipitated in ethanol/hexanes (50:50, v/v). The precipitate was washed repeatedly with water until the residual water was pH 7 and then dried under vacuum at 60 °C for 24 h. The ^{1}H NMR spectra of the sulfonated polymers showed similar signature peaks to that of the pristine polymers, except an additional peak at 7.8−7.4 ppm, which is related to aromatic protons adjacent to the sulfonate group.

Membrane Preparation and Characterization. Membranes were prepared by dissolving the sulfonated diblock copolymers in THF, drop-casting on a leveled Teflon sheet, and immediately covering the film with a Petri dish to slow down the solvent evaporation. Polymer membranes were dried at room temperature for 2 h, and then at 60 °C under vacuum for 24 h. The membranes (∼100 μm thick) were protonated by immersing in 2 M HCl for 24 h. The protonated membranes were washed several times with Milli-Q water for 30 min periods and stored in water for 24 h to remove excess acid on the surface and interior of the membranes.

The pretreated membranes (protonic form) were equilibrated in 2 M NaCl for at least 4 h to release the protons, which were subsequently titrated with 0.025 M NaOH to a phenolphthalein end point. Acid−base control titrations were performed on 2 M NaCl solutions with no

membranes present to determine the "blank" titration volume. Following titration, the membranes were reprotonated by immersing in 2 M HCl for a minimum of 4 h. After drying at 80 °C under vacuum for 24 h, the membranes "dry" weights were measured. The ion exchange capacity (IEC, mmol/g) of the membrane was calculated by

$$\text{IEC} = \frac{V_{\text{NaOH}} M_{\text{NaOH}}}{W_{\text{dry}}} \quad (4)$$

where V_{NaOH} and M_{NaOH} are the blank-corrected volume (mL) and molar concentration (mol/L) of the NaOH titrant, respectively. W_{dry} is the dry weight of the membrane.

The membranes were equilibrated in Milli-Q deionized water for 24 h and blotted with a Kimwipe to remove surface water prior to determining the "wet" weight. The water uptake was calculated as the percentage increase in mass over the "dry" weight as follows

$$\text{water uptake} = \frac{W_{\text{wet}} - W_{\text{dry}}}{W_{\text{dry}}} \times 100\% \quad (5)$$

where W_{wet} and W_{dry} are the wet and dry weight of the membrane, respectively.

The water content was calculated both as a mass and a volume percentage of the water in the "wet" membrane and given by

$$\text{water content (wt \%)} = \frac{W_{\text{wet}} - W_{\text{dry}}}{W_{\text{wet}}} \times 100\% \quad (6)$$

$$\text{water content (vol \%)} = X_{\text{v}} = \frac{\text{Vol}_{\text{wet}} - \text{Vol}_{\text{dry}}}{\text{Vol}_{\text{wet}}} \quad (7)$$

where Vol_{wet} and Vol_{dry} are the wet and dry volume of the membrane, respectively. The length and width were measured with a Mitutoyo Digimatic caliper while the thickness was measured using Series 293 Mitutoyo Quickmike thickness micrometer.

IEC, water uptake, and water content were taken as the average values of at least five membrane samples.

Water sorption was also expressed as the average number of water molecules per ion exchange site ($[H_2O]/[SO_3^-]$), often referred to as λ value, and calculated by

$$[H_2O]/[SO_3^-] = \lambda = \frac{\text{water uptake (\%)} \times 10}{18 \times \text{IEC (mmol/g)}} \quad (8)$$

The analytical acid concentration in "wet" membrane was given by

$$[-SO_3H] = \frac{W_{\text{dry}}\,(\text{g})}{\text{Vol}_{\text{wet}}\,(\text{cm}^3)} \times \text{IEC (mmol/g)} \quad (9)$$

The *effective* proton mobility in "wet" membranes (μ_{eff}) was calculated by

$$\mu_{\text{eff}} = \frac{\sigma}{F \times [-SO_3H]} \quad (10)$$

where F is Faraday's constant and σ (S/cm) is the proton conductivity.

Instrumentation and Techniques. The molecular weights of the fluorous macroinitiator and the diblock copolymers were estimated by gel permeation chromatography (GPC) using three Waters Styragel HT columns at 25 °C, a Waters 1515 isocratic HPLC pump, THF eluant, a Waters 2414 differential refractometer, and a Waters 2487 dual UV absorbance detector (λ = 254 nm). Polystyrene standards were used for calibration. ^{1}H NMR spectra (in acetone-d_6) were recorded on a 500 MHz Varian Inova spectrometer. ^{19}F NMR spectra (in acetone-d_6) were recorded on a 400 MHz Varian MercuryPlus spectrometer, and chemical shifts were measured with respect to trichlorofluoromethane ($CFCl_3$).

In-plane and *through-plane* proton conductivities were measured by ac impedance spectroscopy with a Solartron 1260 frequency response analyzer (FRA) employing a two-probe electrochemical cell. Detailed procedures of the method is described elsewhere.[69,71] A 100 mV sinusoidal ac voltage over a frequency range of 10 MHz to 100 Hz was applied to obtain Nyquist plots. Data was analyzed using commercial *Z* plot/*Z* view software (Scribner Associates).

In the case of in-plane proton conductivity, a strip of membrane (10 mm ×5 mm) was placed between two Pt electrodes (~5 mm apart, fixed in place by attaching them to an inert Teflon block). Another Teflon block was placed on top and tightened to immobilize the membrane while an alternating current was passed along the plane of the sample. The resulting Nyquist plots were fitted to a Randles equivalent circuit consisting of an interfacial contact resistance (R_c) acting in series with a parallel combination of a membrane bulk capacitance (C_m) and a membrane bulk resistance (R_m), as shown below:

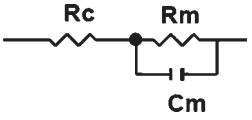

In-plane proton conductivity ($\sigma_{\parallel}$) was calculating by

$$\sigma = \frac{L}{RA} \quad (11)$$

where L (cm) is the distance between Pt electrodes, R (Ω) is the membrane resistance, and A (cm^2) is the cross-sectional area of the membrane.

For through-plane conductivity measurements, membranes (5 mm × 5 mm) were sandwiched between two Pt electrodes, and the electrochemical cells were tightened with screws. Prior to conducting the measurements, the cell was calibrated to determine the high frequency inductance of the cell by measuring the impedances of the shorted cell and the "opened" cell. Both data files were saved and subsequently used as nulling (i.e., background) files in the Z plot software. Membrane resistances were obtained by fitting the Nyquist plots into an equivalent circuit comprising of an interfacial double-layer capacitance (C_{dl}) acting in series with a parallel combination of C_m and R_m:

Through-plane conductivity ($\sigma_{\perp}$) was also calculated using the eq 11 except that L (cm) is the thickness of the membrane and A (cm^2) is the area of the Pt electrode. Conductivity values were reported as averages of at least five membrane samples.

The degree of conductivity anisotropy is calculated by

$$\sigma_{\parallel/\perp} = \frac{\sigma_{\parallel}}{\sigma_{\perp}} \quad (12)$$

where $\sigma_{\parallel/\perp}$ is the proton conductivity anisotropy, $\sigma_{\parallel}$ is the in-plane conductivity (average of X and Y directions) and $\sigma_{\perp}$ is the through-plane conductivity (Z direction).

Samples for transmission electron microscopy (TEM) were prepared as follows: membranes were stained by immersing in a saturated lead acetate solution for 12 h, then rinsed repeatedly in water, and dried at room temperature under vacuum for 4 h. The stained membranes were embedded in Spurr's epoxy and cured for 6 h in a oven at 60 °C. The samples were sectioned to yield slices ~100 nm thick using a Leica UC6 ultramicrotome and picked up on copper grids. Electron micrographs

were taken with a Hitachi H7600 TEM using an accelerating voltage of 80 kV.

■ ASSOCIATED CONTENT

Supporting Information. GPC traces, ^{19}F NMR spectra and membrane properties. This material is available free of charge via the Internet at http://pubs.acs.org/.

■ AUTHOR INFORMATION

Corresponding Author

*E-mail: holdcrof@sfu.ca.

Present Addresses

†Institute for Fuel Cell Innovation, National Research Council Canada, 4250 Wesbrook Mall, Vancouver, BC V6T 1W5, Canada

■ ACKNOWLEDGMENT

The authors thank the Natural Sciences and Engineering Research Council of Canada (NSERC) for financial support.

■ REFERENCES

(1) Vielstich, W.; Lamm, A.; Gasteiger, H. A., *Handbook of Fuel Cells-Fundamentals, Technology and Applications*; Wiley: New York, 2003.
(2) Hickner, M. A.; Ghassemi, H.; Kim, Y. S.; Einsla, B. R.; McGrath, J. E. *Chem. Rev.* **2004**, *104*, 4587–4611.
(3) Smitha, B.; Sridhar, S.; Khan, A. A. *J. Membr. Sci.* **2005**, *259*, 10–26.
(4) Rikukawa, M.; Sanui, K. *Prog. Polym. Sci.* **2000**, *25*, 1463–1502.
(5) Hamrock, S. J.; Yandrasits, M. A. *Polym. Rev.* **2006**, *46*, 219–244.
(6) Li, Q.; He, R.; Jensen, J. O.; Bjerrum, N. J. *Chem. Mater.* **2003**, *15*, 4896–4915.
(7) Miyatake, K.; Watanabe, M. *Electrochem. (Jpn.)* **2005**, *73*, 12–19.
(8) Kreuer, K. D. *J. Membr. Sci.* **2001**, *185*, 29–39.
(9) Yang, Y.; Holdcroft, S. *Fuel Cells* **2005**, *5*, 171–186.
(10) Peckham, T. J.; Holdcroft, S. *Adv. Mater.* **2010**, *22*, 4667–4690.
(11) Yang, Y. S.; Siu, A.; Peckham, T. J.; Holdcroft, S. *Fuel Cells I*; Springer-Verlag: Berlin, 2008; Vol. 215, pp 55−126.
(12) Gebel, G. *Polymer* **2000**, *41*, 5829–5838.
(13) Gebel, G.; Aldebert, P.; Pineri, M. *Polymer* **1993**, *34*, 333–339.
(14) Gebel, G.; Lambard, J. *Macromolecules* **1997**, *30*, 7914–7920.
(15) Rollet, A. L.; Diat, O.; Gebel, G. *J. Phys. Chem. B* **2002**, *106*, 3033–3036.
(16) Schmidt-Rohr, K.; Chen, Q. *Nat. Mater.* **2008**, *7*, 75–83.
(17) Mauritz, K. A.; Moore, R. B. *Chem. Rev.* **2004**, *104*, 4535–4585.
(18) Bates, F. S.; Fredrickson, G. H. *Annu. Rev. Phys. Chem.* **1990**, *41*, 525–557.
(19) Bates, F. S.; Schulz, M. F.; Khandpur, A. K.; Forster, S.; Rosedale, J. H.; Almdal, K.; Mortensen, K. *Faraday Discuss.* **1994**, *98*, 7–18.
(20) Elabd, Y. A.; Hickner, M. A. *Macromolecules* **2011**, *44*, 1–11.
(21) Weiss, R. A.; Sen, A.; Pottick, L. A.; Willis, C. L. *Polymer* **1991**, *32*, 2785–2792.
(22) Weiss, R. A.; Sen, A.; Willis, C. L.; Pottick, L. A. *Polymer* **1991**, *32*, 1867–1874.
(23) Lu, X. Y.; Steckle, W. P.; Weiss, R. A. *Macromolecules* **1993**, *26*, 6525–6530.
(24) Lu, X. Y.; Steckle, W. P.; Weiss, R. A. *Macromolecules* **1993**, *26*, 5876–5884.
(25) Lu, X. Y.; Steckle, W. P.; Hsiao, B.; Weiss, R. A. *Macromolecules* **1995**, *28*, 2831–2839.
(26) Edmondson, C. A.; Fontanella, J. J.; Chung, S. H.; Greenbaum, S. G.; Wnek, G. E. *Electrochim. Acta* **2001**, *46*, 1623–1628.
(27) Kim, J.; Kim, B.; Jung, B. *J. Membr. Sci.* **2002**, *207*, 129–137.
(28) Kim, J.; Kim, B.; Jung, B.; Kang, Y. S.; Ha, H. Y.; Oh, I. H.; Ihn, K. J. *Macromol. Rapid Commun.* **2002**, *23*, 753–756.
(29) Mauritz, K. A.; Storey, R. F.; Mountz, D. A.; Reuschle, D. A. *Polymer* **2002**, *43*, 4315–4323.
(30) Mauritz, K. A.; Storey, R. F.; Reuschle, D. A.; Tan, N. B. *Polymer* **2002**, *43*, 5949–5958.
(31) Lee, W. J.; Jung, H. R.; Lee, M. S.; Kim, J. H.; Yang, K. S. *Solid State Ion.* **2003**, *164*, 65–72.
(32) Won, J.; Choi, S. W.; Kang, Y. S.; Ha, H. Y.; Oh, I. H.; Kim, H. S.; Kim, K. T.; Jo, W. H. *J. Membr. Sci.* **2003**, *214*, 245–257.
(33) Won, J.; Kang, Y. S. *Macromol. Symp.* **2003**, *204*, 79–91.
(34) Kim, B.; Kim, J.; Jung, B. *J. Membr. Sci.* **2005**, *250*, 175–182.
(35) Mauritz, K. A.; Blackwell, R. I.; Beyer, F. L. *Polymer* **2004**, *45*, 3001–3016.
(36) Storey, R. F.; Chisholm, B. J.; Masse, M. A. *Polymer* **1996**, *37*, 2925–2938.
(37) Elabd, Y. A.; Napadensky, E.; Sloan, J. M.; Crawford, D. M.; Walker, C. W. *J. Membr. Sci.* **2003**, *217*, 227–242.
(38) Elabd, Y. A.; Walker, C. W.; Beyer, F. L. *J. Membr. Sci.* **2004**, *231*, 181–188.
(39) Elabd, Y. A.; Napadensky, E. *Polymer* **2004**, *45*, 3037–3043.
(40) Elabd, Y. A.; Napadensky, E.; Walker, C. W.; Winey, K. I. *Macromolecules* **2006**, *39*, 399–407.
(41) Mokrini, A.; Acosta, J. L. *Polymer* **2001**, *42*, 9–15.
(42) Mokrini, A.; Del Rio, C.; Acosta, J. L. *Solid State Ion.* **2004**, *166*, 375–381.
(43) Mani, S.; Weiss, R. A.; Williams, C. E.; Hahn, S. F. *Macromolecules* **1999**, *32*, 3663–3670.
(44) Saito, T.; Moore, H. D.; Hickner, M. A. *Macromolecules* **2010**, *43*, 599–601.
(45) Park, M. J.; Balsara, N. P. *Macromolecules* **2008**, *41*, 3678–3687.
(46) Park, M. J.; Balsara, N. P. *Macromolecules* **2010**, *43*, 292–298.
(47) Chen, L.; Hallinan, D. T.; Elabd, Y. A.; Hillmyer, M. A. *Macromolecules* **2009**, *42*, 6075–6085.
(48) Trabelsi, H.; Szonyi, S.; Gaysinski, M.; Cambon, A.; Watzke, H. J. *Langmuir* **1993**, *9*, 1201–1205.
(49) Shi, Z. Q.; Holdcroft, S. *Macromolecules* **2004**, *37*, 2084–2089.
(50) Shi, Z. Q.; Holdcroft, S. *Macromolecules* **2005**, *38*, 4193–4201.
(51) Tsang, E. M. W.; Zhang, Z.; Shi, Z.; Soboleva, T.; Holdcroft, S. *J. Am. Chem. Soc.* **2007**, *129*, 15106–15107.
(52) Rubatat, L.; Shi, Z. Q.; Diat, O.; Holdcroft, S.; Frisken, B. J. *Macromolecules* **2006**, *39*, 720–730.
(53) Kotani, Y.; Kato, M.; Kamigaito, M.; Sawamoto, M. *Macromolecules* **1996**, *29*, 6979–6982.
(54) Destarac, M.; Matyjaszewski, K.; Silverman, E.; Ameduri, B.; Boutevin, B. *Macromolecules* **2000**, *33*, 4613–4615.
(55) Semsarzadeh, M. A.; Mirzaei, A.; Vasheghani-Farahani, E.; Haghighi, M. N. *Eur. Polym. J.* **2003**, *39*, 2193–2201.
(56) Isbester, P. K.; Brandt, J. L.; Kestner, T. A.; Munson, E. J. *Macromolecules* **1998**, *31*, 8192–8200.
(57) ChemDraw Ultra software version 8.0, CambridgeSoft Corporation
(58) Ding, J. F.; Chuy, C.; Holdcroft, S. *Macromolecules* **2002**, *35*, 1348–1355.
(59) Ding, J. F.; Chuy, C.; Holdcroft, S. *Adv. Funct. Mater.* **2002**, *12*, 389–394.
(60) Khandpur, A. K.; Forster, S.; Bates, F. S.; Hamley, I. W.; Ryan, A. J.; Bras, W.; Almdal, K.; Mortensen, K. *Macromolecules* **1995**, *28*, 8796–8806.
(61) Matsen, M. W.; Bates, F. S. *Macromolecules* **1996**, *29*, 1091–1098.
(62) Lu, X. Y.; Weiss, R. A. *Macromolecules* **1996**, *29*, 1216–1221.
(63) Eisenberg, A.; Hird, B.; Moore, R. B. *Macromolecules* **1990**, *23*, 4098–4107.
(64) Yarusso, D. J.; Cooper, S. L. *Macromolecules* **1983**, *16*, 1871–1880.
(65) Won, J.; Park, H. H.; Kim, Y. J.; Choi, S. W.; Ha, H. Y.; Oh, I. H.; Kim, H. S.; Kang, Y. S.; Ihn, K. J. *Macromolecules* **2003**, *36*, 3228–3234.

(66) Tsang, E. M. W.; Zhang, Z. B.; Yang, A. C. C.; Shi, Z. Q.; Peckham, T. J.; Narimani, R.; Frisken, B. J.; Holdcroft, S. *Macromolecules* **2009**, *42*, 9467–9480.
(67) Gavach, C.; Pamboutzoglou, G.; Nedyalkov, M.; Pourcelly, G. *J. Membr. Sci.* **1989**, *45*, 37–53.
(68) Peckham, T. J.; Schmeisser, J.; Rodgers, M.; Holdcroft, S. *J. Mater. Chem.* **2007**, *17*, 3255–3268.
(69) Soboleva, T. Y.; Xie, Z.; Shi, Z. Q.; Tsang, E.; Navessin, T. C.; Holdcroft, S. *J. Electroanal. Chem.* **2008**, *622*, 145–152.
(70) Blachot, J. F.; Diat, O.; Putaux, J. L.; Rollet, A. L.; Rubatat, L.; Vallois, C.; Muller, M.; Gebel, G. *J. Membr. Sci.* **2003**, *214*, 31–42.
(71) Xie, Z.; Song, C. J.; Andreaus, B.; Navessin, T.; Shi, Z. Q.; Zhang, J. J.; Holdcroft, S. *J. Electrochem. Soc.* **2006**, *153*, E173–E178.